Veterinary Radiology & Ultrasound

WILEY

ORIGINAL RESEARCH OPEN ACCESS

Short/Ultra-Short TE MRI Sequences Comparable to CT and Superior to Standard MRI Sequences for Canine Skull Imaging

Maura C. Cicci[1,2] | Erin K. Keenihan[2] | Kate Bailey[2] | Lynelle Graham[2] | Stefan Sommer[3,4,5] | Eli B. Cohen[2,6]

[1]Red Bank Veterinary Hospital, Tinton Falls, New Jersey, USA | [2]Department of Molecular Biomedical Sciences, College of Veterinary Medicine, NC State University, Raleigh, North Carolina, USA | [3]Siemens Healthcare AG, Zurich, Switzerland | [4]Swiss Center for Musculoskeletal Imaging (SCMI), Zurich, Switzerland | [5]Advanced Clinical Imaging Technology (ACIT), Siemens Healthcare AG, Lausanne, Switzerland | [6]Dragonfly Imaging, PLLC, Cary, North Carolina, USA

Correspondence: Eli B. Cohen (ecohen@dragonflyimaging.vet)

Received: 17 April 2024 | **Revised:** 26 March 2025 | **Accepted:** 13 April 2025

Keywords: bone imaging | PETRA | UTE | VIBE

ABSTRACT

Magnetic resonance imaging often needs to be complemented with CT for complete assessment of bony structures due to CTs increased spatial resolution and discrimination of cortical bone margins. The aims of this prospective method comparison study were to perform qualitative and quantitative comparisons of standard MR sequences with three short/ultra-short TE MR sequences using CT as the gold standard. Eight healthy research dogs of similar size had CT and MR of the head performed. Three short/ultra-short TE sequences, VIBE, PETRA, and UTE, alongside standard T2W, PD, and T1W TSE sequences of the head were obtained. Slice thickness of CT and short TE MR sequences were matched. A qualitative scale was used to assess the visibility of cortical margins and skull foramina. For the quantitative assessment, predetermined osseous structures and foramina on designated slices were measured. Levene's test and post hoc folded *F* tests with false discovery rate adjustments were applied to the residuals from these models to compare precision relative to CT across the sequence types. The short/ultra-short TE MR sequences were significantly better than the standard MR sequences for quantitative assessment of bone thickness of smaller structures and overall qualitative assessment. Any of these short/ultra-short TE sequences may be viable to incorporate into a clinical setting as an alternative to CT to help further evaluate the skull and reduce anesthesia time and client cost. VIBE, PETRA, and UTE sequences have diagnostic image quality and provide a consistent quantitative and qualitative assessment of the cortical bone of the skull when compared with CT.

1 | Introduction

Magnetic resonance imaging is the gold standard imaging modality for evaluating the nervous system due to its superior soft tissue contrast resolution. Magnetic resonance bone imaging is increasingly becoming a focus of interest in the human medical field [1]. Assessment of cortical bone can be difficult and/or nondiagnostic in MR due to cortical bone having a low proton density and a very short T2 relaxation time, resulting in low signal on conventional sequences [1, 2]. In conventional MR sequences, the minimally achievable TE for the spin-echo and gradient-echo pulse sequences is too long to detect a significant signal from the bone [1, 2]. In most clinical cases, CT is the gold standard for the evaluation of cortical bone due to its high spatial resolution and lack of artifact (e.g., at interfaces with gas). Whilst CT is often utilized in trauma situations, particularly of the abdomen and

thorax, inferior soft tissue contrast resolution in CT compared with MR hampers the detailed assessment of some soft tissue structures, particularly those within the skull and vertebral canal. As such, MR and CT often need to be paired together to provide complete diagnostic information on both the skull and brain, particularly in trauma patients. This is suboptimal, as it results in additional transport, repositioning, and anesthetic time in often unstable patients, increased cost to the client, and delay of intervention/surgery when indicated. A recent retrospective veterinary study compared MRI and CT in the evaluation of vertebral fractures and found limited agreement between the two modalities. However, this study only evaluated standard MR sequences (T2W, T2*, T1W) [3].

In human medicine, MR sequences specifically designed for bone imaging, including 3D gradient echo, zero TE (ZTE), and ultra-short TE (UTE) techniques with the addition of nontraditional k-space filling, have been described and validated against CT as the gold standard [1, 4–8]. The implementation of these sequences in human medicine has shown excellent bone image quality and the potential to avoid additional CT examinations [1, 4–7]. This streamlined workflow can allow for a reduction of radiation exposure and reduced cost [8]. If validated in veterinary patients, similar benefits in addition to reduced anesthetic time could be realized.

Volumetric interpolated breath-hold examination (VIBE) is a 3D gradient-echo MR sequence. T1-weighted VIBE can be utilized to clearly define cortical bone anatomy when surrounded by fat and muscle and produce CT-like images [7]. Pointwise encoding time reduction with radial acquisition (PETRA) is a hybrid sequence that combines features of single-point imaging with radial center-out readout trajectories [9]. The signal is acquired with near-zero echo time after the application of the RF pulse, and filling up k-space in a radial fashion creates imaging at isotropic resolution [11]. UTE also uses very short TE values between 9 and 500 ms. However, no single-point imaging is needed in comparison to the PETRA sequence. Some UTE sequence implementations allow for long T2 suppression, for example, by subtraction of a second echo, which can improve the discrimination of bone from soft tissue [1, 2, 10].

The utilized UTE prototype sequence uses a hard RF block pulse followed by a 3D radial center-out trajectory. An additional echo can be acquired optionally with a rewinder gradient and additional center-out acquisition. Like the PETRA sequence, the non-Cartesian k-space data needs to be reconstructed by a nonuniform Fourier transform using gridding, resulting in images with isotropic resolution.

The purpose of our study was to determine if short TE MR sequences specific for bone imaging (VIBE, PETRA, UTE) can produce images of diagnostic quality comparable to CT, and superior to standard MR sequences (T2W, PD, T1W) in terms of bone assessment. This study aimed to perform qualitative and quantitative comparisons of standard MR sequences with the three short/ultra-short TE MR sequences using CT as the gold standard. We hypothesized that the short/ultra-short TE sequences would provide similar qualitative and quantitative image quality regarding cortical bone and associated anatomy compared with CT and would provide superior visibility and image quality of cortical bone and associated anatomy compared with standard MR sequences. We also hypothesized that the standard MR sequences would produce inferior diagnostic images for evaluating cortical bone and associated anatomy compared with CT.

2 | Materials and Methods

2.1 | Selection and Description of Subjects

This prospective method comparison study was approved by and conducted in accordance with the Institutional Animal Care and Use Committee (IACUC) at North Carolina State University's College of Veterinary Medicine. Eight healthy research hound dogs of similar size (average weight 19.1 kg) were used for imaging. Dogs were classified as healthy based on no history of illness, normal physical examination, normal serum chemistry, and complete blood count. Two board-certified veterinary anesthesiologists (L. G. and K. B.) performed and monitored all sedation and anesthesia for the duration of the study.

2.2 | Imaging Acquisition

The CT images were acquired under sedation, in sternal recumbency, using a multislice CT scanner (SOMATOM Perspective 64 slice, Siemens Medical Solution, Malvern, PA) and a standard CT skull protocol was acquired (kV: 130, mA:25, slice thickness 0.6 mm). Images were reconstructed in a bone algorithm in the transverse plane, with subsequent dorsal and sagittal plane reconstructions created in viewing software (Horos, Version 3.3.6, Horos Project, Annapolis, MD, USA).

For MR imaging, each anesthetized dog was placed in dorsal recumbency in a 3 Tesla scanner (MAGNETOM Skyra, Siemens Healthcare, Erlangen, Germany). Depending on the dog's size, either a 15-channel knee coil or an 18-channel body flex coil was used. T2-weighted (transverse, sagittal, dorsal), T1-weighted fluid-attenuated inversion recovery with fat saturation (T1-FLAIR FS) (transverse, dorsal), PD (transverse, dorsal), VIBE, PETRA, and UTE prototype sequences were acquired (see Table 1 for imaging parameters).

2.3 | Data Recording and Analysis

The veterinary radiology resident (M. C. C.), one ACVR-certified radiologist (E.B.C.), and one ECVDI-certified radiologist (E. K. K.) reached a consensus on both qualitative and quantitative assessments. CT was used as the gold standard for evaluation. For the quantitative assessment, predetermined osseous structures and foramina on matched CT and MR slices were measured in each dog for either overall thickness or diameter (see Addendum 1 for structures evaluated and Figure 1). The quantitative data were divided into three categories: overall bone thickness, intracranial dimensions, and foraminal measurements. For the qualitative assessment, visibility of cortical margins, distinction between bone and adjacent soft tissue structures/gas, and visibility of skull foramina at predetermined sites on matched CT and MR slices were assessed in each dog (see Addendum 2 for structures

TABLE 1 | MR sequences and imaging parameters for evaluation of the canine skull.

Parameter	T2W sagittal dorsal	T2W transverse	T1 FLAIR FS transverse	T1 FLAIR FS dorsal	PD transverse	PD dorsal	T1 VIBE transverse	PETRA transverse	UTE transverse
TE (ms)	107	107	8.2	8.5	10	11	4.2	0.07	0.04
TR (ms)	2830	3430	2060	2290	2860	2770	8.72	7	8.58 (20 segments)
Number of signals averaged	1	1	2	2	1	1	2	1	1
Slice thickness (mm)	2.5	3.0	3.0	2.5	3.0	2.5	0.59	0.56	0.57
Acquisition matrix	205 × 256	205 × 256	192 × 256	192 × 256	205 × 256	205 × 256	384 × 384	Base 416 × 96,000 radial views	Base 384 × 64,980 radial views
Flip angle	120	120	120	120	160	160	5	2	5
Field of view (mm^2)	150	150	150	150	150	150	220	235	220
Time (min)	2–3	5–6	4–5	3–4	5–6	4–5	16–17	9–10	10–11

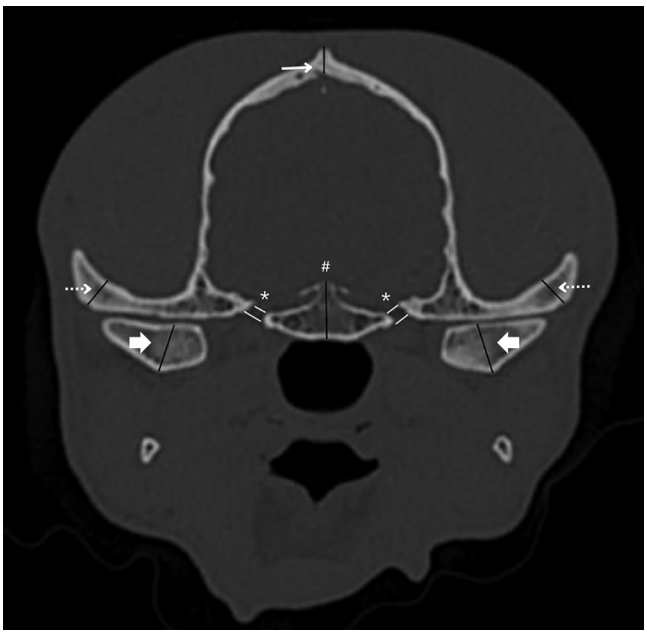

FIGURE 1 | Transverse CT image with quantitative bone thickness measurements. Measurements at this level include bilateral oval foramen, inner and outer widths at the largest dimensions (*); bilateral zygomatic process of the temporal bone, perpendicular to the bone at the widest part at the level of the temporomandibular joint (dotted arrow); external sagittal crest of the parietal bone, dorsoventral measurement at the level of the sagittal suture (plain arrow); bilateral condylar process of the mandible, perpendicular to the bone at the widest part at the level of the temporomandibular joint (block arrow); basisphenoid bone, dorsoventral measurement including the dorsum sellae (#).

evaluated), using a scale of 0 = not visible, 1 = partially visible, and 2 = visible and distinct from adjacent structures. The qualitative data was divided into two categories: bone evaluation and foramen visibility.

2.4 | Statistics

Statistical analyses were chosen and performed by an experienced statistician with a Ph.D. in statistics. We conducted a power analysis, and we could achieve a power of 0.99 using eight dogs. For quantitative assessment, linear mixed-effects models were used to determine whether there were statistical differences between mean MRI and CT measures; these models accounted for random effects of dog and structure. The models were separated according to structure type (intracranial, foramen, or thickness). Further, to understand how precisely each MRI sequence reproduces CT results, the variability of the differences from CT for each MRI sequence type was summarized based on the results of these models. Levene's test and post hoc folded F tests with false discovery rate (FDR) adjustments for multiple testing were applied to the residuals from these models to compare precision relative to CT across the sequence types. For qualitative assessment, ordinal logistic mixed effects models were used to compare image quality (visibility = 0, 1, 2) of the MRI sequence types to CT scans; these models accounted for random effects of dog and structure. The models were separated according to structure type (intracranial, foramen, or thickness). Post hoc pairwise comparison of odds ratios from these models was used to compare the probability of higher levels of quality between each of the MRI sequences and CT scans; a Tukey adjustment was used for multiple comparisons.

3 | Results

3.1 | Quantitative Assessment

Table 2 shows the mean differences from CT by MRI sequence for intracranial structures from the linear mixed effect models; only T2 is significantly different from CT at the 0.05 level of significance. Table 3 shows the differences from CT by MRI sequence for foramen from the linear mixed effects model;

TABLE 2 | Estimated marginal mean differences from CT by sequence for intracranial structures.

Sequence	Mean difference	Std. error	95% CI (Diff)		*t*	df	*p*
PD	1.22	0.62	−0.05	2.48	1.96	30.3	.059
PETRA	0.62	0.47	−0.39	1.63	1.31	16.1	.209
T1	−0.07	0.62	−1.33	1.19	−0.11	33.2	.911
T2	1.15	0.55	0.02	2.27	2.10	25.9	.046
UTE	0.50	0.48	−0.52	1.52	1.03	17.7	.318
VIBE	0.80	0.47	−0.20	1.80	1.71	14.9	.108

TABLE 3 | Estimated marginal mean differences from CT by sequence for foramen structures.

Sequence	Mean difference	Std. error	95% CI (Diff)		*t*	df	*p*
PD	0.689	0.330	0.017	1.362	2.09	31.6	.045
PETRA	−0.014	0.129	−0.284	0.256	−0.11	19.1	.913
T1	−0.094	0.217	−0.531	0.343	−0.43	46.2	.666
T2	0.929	0.463	−0.020	1.879	2.01	27.6	.055
UTE	0.128	0.131	−0.147	0.402	0.97	19.7	.343
VIBE	0.198	0.122	−0.060	0.456	1.63	16.1	.123

TABLE 4 | Estimated marginal mean differences from CT by sequence for thickness structures.

Sequence	Mean difference	Std. error	95% CI (Diff)		*t*	df	*p*
PD	0.396	0.068	0.262	0.530	5.81	189.0	<.001
PETRA	−0.132	0.044	−0.221	−0.043	−2.99	52.8	.004
T1	0.145	0.052	0.042	0.249	2.80	94.4	.006
T2	0.181	0.077	0.029	0.334	2.35	204.0	.020
UTE	−0.089	0.043	−0.175	−0.003	−2.08	46.2	.043
VIBE	0.009	0.045	−0.082	0.099	0.20	57.3	.845

only PD is significantly different from CT at the 0.05 level of significance. Finally, Table 4 shows the difference for CT by MRI sequence for thickness from the linear mixed effects model; all sequences except VIBE are significantly different from CT at the 0.05 level of significance. The standard MRI sequences tend to be positively biased for thickness, meaning that the estimates of thickness are larger than when using CT. The novel sequences tend to be negatively biased, meaning the estimates of thickness are smaller than when using CT, and the differences also tend to be smaller than for the standard sequences.

To determine which sequences more precisely replicate CT results than others, we use a series of folded *F* tests comparing the residuals from the previous model for the MRI sequences to each other two at a time for all three categories (intracranial, foramen, thickness). Note that precision is different from bias; it is possible for a particular MRI sequence to be biased but still precise if the measures differ from the CT measures by a similar amount every time. This could still be a preferable sequencing approach because an overall adjustment could be made, and the measures would resemble the CT measures very closely. The residuals from the previous model represent the difference between each MRI sequence measurement and the corresponding CT measurement after adjusting for the effects of individual animals and structures. By comparing the variability of these values across MRI sequences, we can determine whether the differences from CT measures are more variable for some sequences than others.

Table 5 shows the model estimated standard deviations of the differences from CT associated with each of the MRI sequences from each model (within dogs and structures). Tables 6, 7, and 8 show the statistical tests comparing these variabilities across sequences for intracranial, foramen, and thickness structures, respectively. In all cases, the variability of PETRA and VIBE around CT measures is significantly smaller than PD, T1, and T2; UTE also has significantly smaller variability around CT measures than PD, T1, and T2 for foramen and thickness (but not

TABLE 5 | Variability of differences from CT by sequence.

Structure type	Sequence	Standard deviation of differences from CT
Intracranial	PD	2.647
	PETRA	1.823
	T1	2.629
	T2	2.606
	UTE	1.940
	VIBE	1.744
Foramen	PD	1.698
	PETRA	0.816
	T1	1.385
	T2	2.352
	UTE	0.810
	VIBE	0.722
Thickness	PD	0.930
	PETRA	0.537
	T1	0.657
	T2	1.013
	UTE	0.480
	VIBE	0.550

TABLE 6 | Folded *F* tests comparing variability of differences from CT by sequence, intracranial.

Comparison	*F*	Num DF	Den DF	FDR adjusted *p*
PD v PETRA	2.17	31	47	.045
PD v T1	1.01	31	31	.969
PD v T2	1.03	31	47	.969
PD v UTE	1.91	31	47	.083
PD v VIBE	2.39	31	47	.039
PETRA v T1	2.14	31	47	.045
PETRA v T2	2.10	47	47	.045
PETRA v UTE	1.14	47	47	.894
PETRA v VIBE	1.10	47	47	.936
T1 v T2	1.02	31	47	.969
T1 v UTE	1.88	31	47	.083
T1 v VIBE	2.35	31	47	.039
T2 v UTE	1.84	47	47	.083
T2 v VIBE	2.31	47	47	.039
UTE v VIBE	1.25	47	47	.665

at the 0.05 level for intracranial). PETRA and VIBE (and UTE for foramen and thickness), therefore, are significantly more precise approximations of CT than the standard MR sequences.

TABLE 7 | Folded *F* tests comparing variability of differences from CT by sequence, foramen.

Comparison	*F*	Num DF	Den DF	*p*
PD v PETRA	4.43	28	71	<.001
PD v T1	1.51	28	48	.259
PD v T2	1.92	26	28	.127
PD v UTE	4.5	28	66	<.001
PD v VIBE	5.72	28	69	<.001
PETRA v T1	2.94	48	71	<.001
PETRA v T2	8.52	26	71	<.001
PETRA v UTE	1.02	71	66	.948
PETRA v VIBE	1.29	71	69	.333
T1 v T2	2.9	26	48	.002
T1 v UTE	2.98	48	66	<.001
T1 v VIBE	3.79	48	69	<.001
T2 v UTE	8.66	26	66	<.001
T2 v VIBE	10.99	26	69	<.001
UTE v VIBE	1.27	66	69	.352

TABLE 8 | Folded *F* tests comparing variability of differences from CT by sequence, thickness.

Comparison	F	Num DF	Den DF	FDR adjusted *p*
PD v PETRA	3.06	254	376	<.001
PD v T1	2.02	254	293	<.001
PD v T2	1.19	218	254	.199
PD v UTE	3.86	254	361	<.001
PD v VIBE	2.91	254	360	<.001
PETRA v T1	1.51	293	376	<.001
PETRA v T2	3.64	218	376	<.001
PETRA v UTE	1.26	376	361	.031
PETRA v VIBE	1.05	360	376	.627
T1 v T2	2.4	218	293	<.001
T1 v UTE	1.91	293	361	<.001
T1 v VIBE	1.44	293	360	.001
T2 v UTE	4.59	218	361	<.001
T2 v VIBE	3.46	218	360	<.001
UTE v VIBE	1.33	360	361	.009

3.2 | Qualitative Assessment

For qualitative bone evaluation, because there was no variability in the outcome for CT (all quality outcomes were a 2), one of the CT outcomes was randomly chosen to be changed to a 1 to allow for statistical analysis to take place. While this does induce some slight bias in the probability of a CT result receiving a perfect

TABLE 9 | Probability of quality rating of 2 by sequence, bone evaluation.

Sequence	Prob(2)	95% CI (Prob(2))	
CT	0.994	0.947	0.999
PETRA	0.973	0.898	0.993
UTE	0.838	0.641	0.937
VIBE	0.823	0.619	0.930
T1	0.137	0.051	0.319
PD	0.108	0.040	0.260
T2	0.091	0.033	0.224

TABLE 10 | Statistical tests comparing quality ratings of sequences, bone evaluation.

Comparison	$\chi^2(1)$	*p*
CT—PETRA	1.72	.847
CT—UTE	10.17	.024
CT—VIBE	10.82	.017
CT—T1	38.50	<.001
CT—PD	41.75	<.001
CT—T2	44.01	<.001
PETRA—UTE	9.01	.043
PETRA—VIBE	10.06	.025
PETRA—T1	60.16	<.001
PETRA—PD	67.02	<.001
PETRA—T2	71.70	<.001
UTE—VIBE	0.05	1.000
UTE—T1	46.54	<.001
UTE—PD	55.53	<.001
UTE—T2	61.83	<.001
VIBE—T1	44.91	<.001
VIBE—PD	53.90	<.001
VIBE—T2	60.21	<.001
T1—PD	0.38	.996
T1—T2	1.11	.941
PD—T2	0.20	.999

quality score, due to the large number of data points, the bias is slight. This also allows the comparison of the MRI sequences to CT quality with only a very small bias.

Table 9 shows the estimated probabilities of achieving a 2 (highest quality) for each sequence for bone evaluation for the model, in order from most to least likely. Table 10 shows the post hoc comparisons comparing the probability of having a higher quality rating across all sequences. There is no statistically significant difference between the quality of CT and PETRA at the 0.05 level; all other sequences are significantly different from CT (all have lower probabilities of higher quality). Among the MRI sequences, all the novel sequences have significantly better quality than PD, T1, and T2 at the 0.05 level. Among the novel sequences, PETRA has significantly better quality than UTE and VIBE; there is not a statistically significant difference between UTE and VIBE at the 0.05 level.

TABLE 11 | Probability of quality rating of 2 by sequence, foramen.

Sequence	Prob(2)	95% CI	(Prob(2))
CT	0.944	0.674	0.993
PETRA	0.944	0.674	0.993
UTE	0.944	0.674	0.993
VIBE	0.944	0.674	0.993
T1	0.277	0.110	0.544
PD	0.174	0.065	0.388
T2	0.080	0.023	0.244

TABLE 12 | Statistical tests comparing quality ratings of sequences, foramen.

Comparison	$\chi^2(1)$	*p*
CT—PETRA	0.00	1.000
CT—UTE	0.00	1.000
CT—VIBE	0.00	1.000
CT—T1	9.93	.027
CT—PD	13.51	.004
CT—T2	17.60	.001
PETRA—UTE	0.00	1.000
PETRA—VIBE	0.00	1.000
PETRA—T1	9.93	.027
PETRA—PD	13.51	.004
PETRA—T2	17.60	.001
UTE—VIBE	0.00	1.000
UTE-T1	9.93	.027
UTE-PD	13.51	.004
UTE-T2	17.60	.001
VIBE-T1	9.93	.027
VIBE-PD	13.51	.004
VIBE-T2	17.60	.001
T1-PD	0.73	.979
T1—T2	3.78	.450
PD—T2	1.59	.870

For qualitative foramen evaluation, which included fewer individual structures, CT, PETRA, UTE, and VIBE all had 2s for all outcomes. This study, therefore, provides no evidence of quality differences between CT and any of the novel sequences. To provide some ability to statistically compare these sequences to the more established MRI sequences, one of each outcome was randomly chosen to be changed to a 1. Table 11 introduces down-

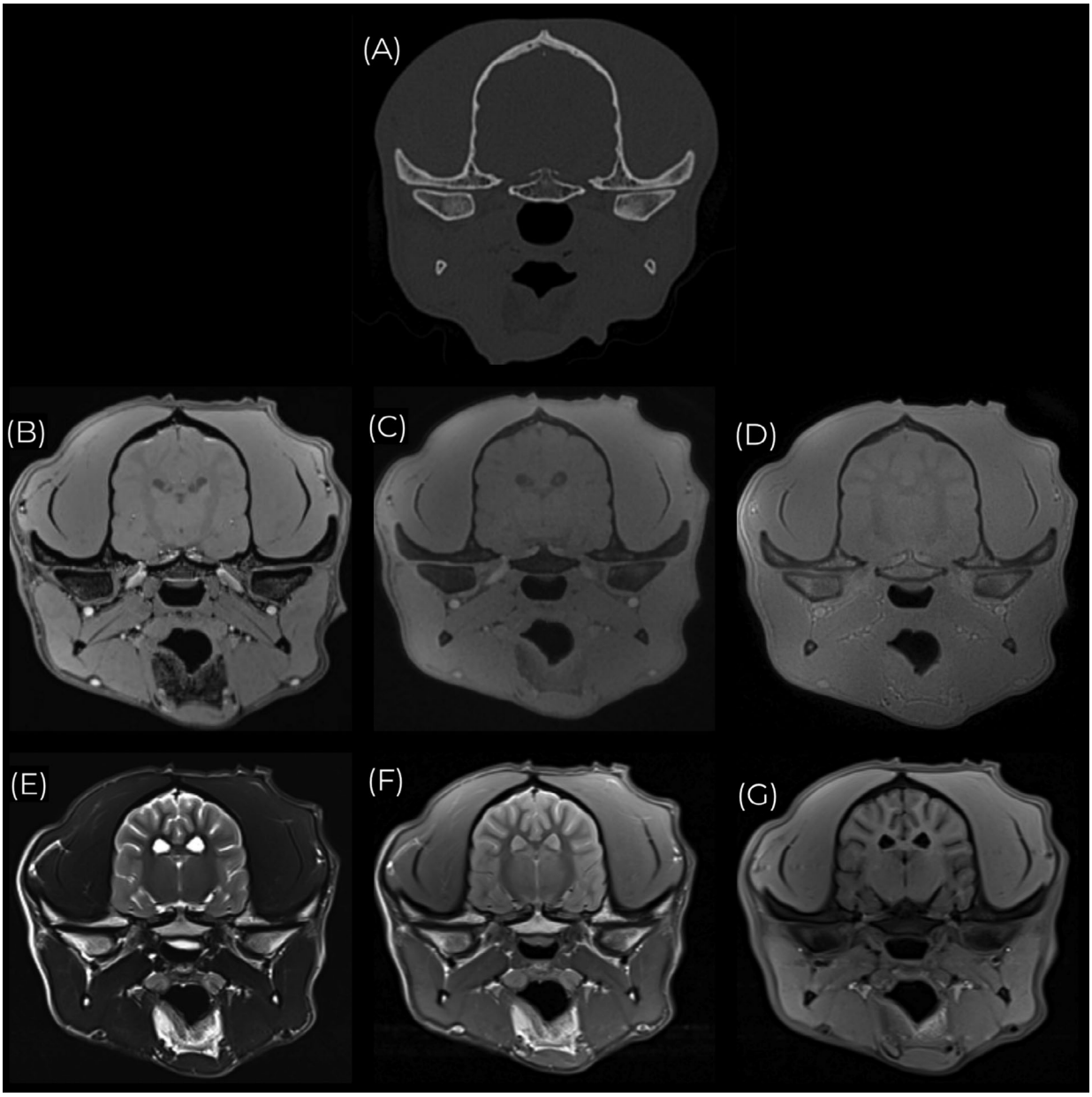

FIGURE 2 | Comparison of CT with ultra-short TE MR Sequences and standard MR images. A, Transverse CT image. B, Transverse VIBE MR image. C, UTE MR image. D, PETRA MR image. E, T2W MR image. F, PD MR image. G, T1W MR image.

ward bias in the estimate of each sequence but is a conservative adjustment that reduces the statistical power of the comparison to the established sequences.

In Table 12, CT and all three of the novel sequences have a model-estimated (downward biased) probability of 94.4% of achieving a 2; PD, T1, and T2 all have lower probabilities of achieving a 2. There were statistically significant differences in quality between CT plus all three of the novel sequences and PD, T1, and T2 at the 0.05 level of significance.

4 | Discussion

The results of our study confirm that short/ultra-short TE MR sequences, specifically VIBE, PETRA, and UTE, provide comparable images to CT and, therefore, could be used in place of CT (Figures 2–4). The addition of either VIBE, PETRA, or UTE sequence could serve as an adjunct to standard MR protocols, allowing for a comprehensive assessment of both soft tissue and osseous structures.

In summary, for intracranial structures, there is no evidence that PETRA, UTE, or VIBE are biased approximations of CT measures. The variability of PETRA and VIBE around CT measures is also significantly smaller than PD, T1, and T2 for intracranial measures. In addition to having larger variability, T2 measures also have significant bias from CT for intracranial measures.

In summary, for foramina, there is no evidence that PETRA, UTE, or VIBE are biased approximations to CT measures. PETRA, VIBE, and UTE all have significantly smaller variability

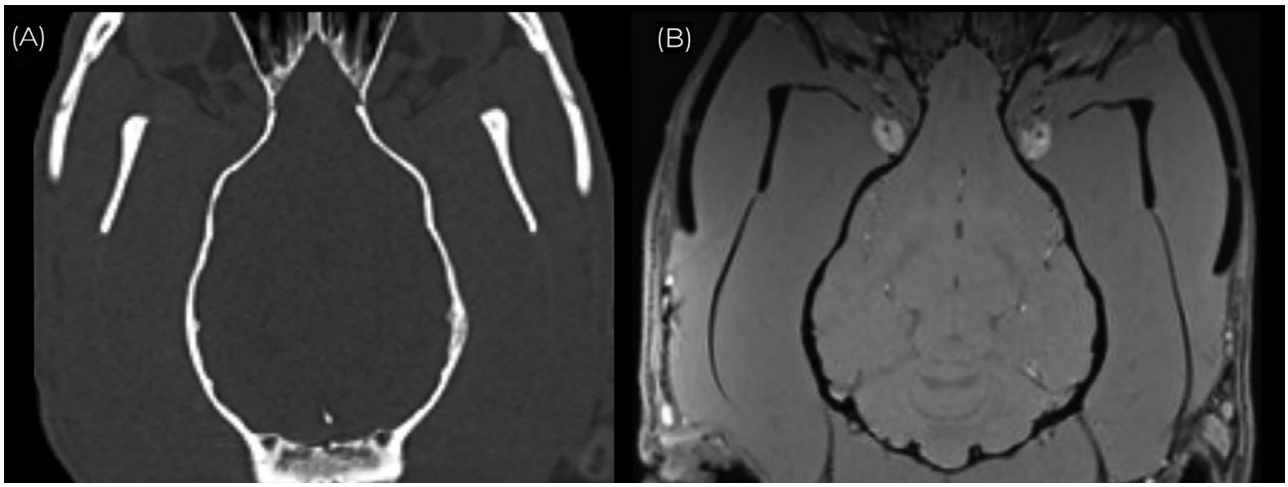

FIGURE 3 | Comparison of dorsal views of CT and VIBE. A, Dorsal CT image. B, Dorsal VIBE image.

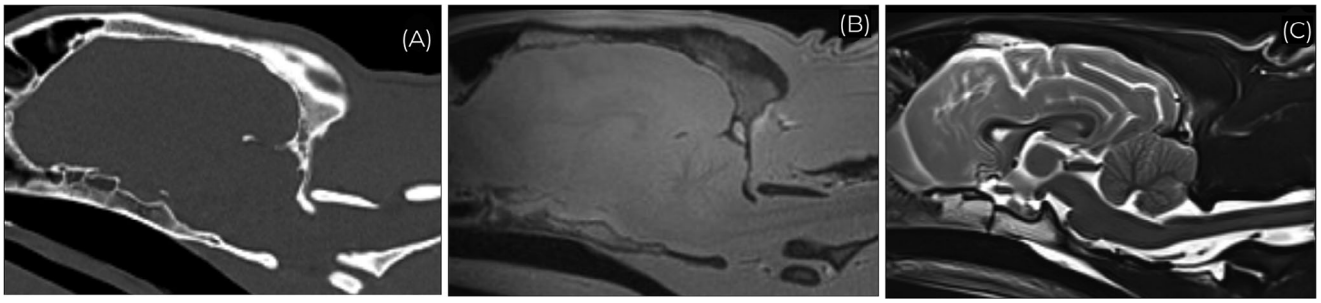

FIGURE 4 | Comparison of Sagittal views of CT, PETRA, and T2W image. A, Sagittal CT image. B, Sagittal PETRA image. C, T2W image.

around CT measures than PD, T1, and T2. In addition to having larger variability, PD measures have significant bias from CT for foramen measures.

In summary, for bone thickness, there is no evidence of bias for VIBE as an approximation of CT measures, while all other sequences (novel and standard) show some significant evidence of bias. However, the variability of PETRA, VIBE, and UTE measures are all significantly smaller than PD, T1, and T2. Despite the bias, UTE also has significantly smaller variability than PETRA or VIBE.

In human medicine, MR bone imaging sequences can negate the need for CT. This results in a reduction of radiation exposure, which is particularly important for radiation-sensitive or young patients. It also reduces costs. Both UTE and ZTE sequences have been validated and routinely used for bone imaging. In our study, we only performed short-TE and UTE sequences due to the availability of these protocols on our MRI machine.

When performing quantitative measurements of the tympanic bulla, it was sometimes difficult to accurately assess and measure cortical margins with the VIBE and UTE sequences because the interface between gas in the tympanic cavity and the adjacent cortical bone of the bulla was not well-defined (Figure 5). In the PETRA sequence, the gas and cortical bone interface was well-defined and allowed for qualitative and quantitative assessment of the tympanic bulla. In a human study using ZTE MR for evaluating segmentation of the skull, air cavity interfaces, such as the inner ear, remained a challenge since bone at bone/fluid interfaces was misclassified as air in regions where bone tissue was too dense to yield sufficient MR signal [8]. In our study, this was only an issue with the measurement of the tympanic bulla. Other bone/gas interfaces, such as the frontal bone adjacent to the frontal sinus and pterygoid bone adjacent to the nasopharynx, were able to be evaluated accurately.

Standard PD weighted sequences have a short TE and long TR and rely on the density of mobile protons and, thus, T2 relaxation of the structure being imaged [12]. PD sequences have been known to be ideal for assessing joints since high mobile proton density structures, such as fluid, have long T2 relaxation times and, thus, a hyperintense signal. Structures with low mobile proton density structures, such as bone and fibrocartilage, have a short T2 relaxation time and, thus, a hypointense signal. When evaluating intracranial measurements, PD performed most comparably to the PETRA and UTE sequences. However, the VIBE was significantly better than the PD.

The addition of these sequences to standard head protocols brings extra imaging/anesthesia time. Scan time for both PETRA and UTE sequences was approximately 10 min, while the VIBE was approximately 16–17 min. Since all short TE sequences were comparable to CT, PETRA or UTE sequences may be the preferred sequence in a clinical setting, given the shorter scan time compared with the VIBE. Even though all the short TE MR sequences are longer than a CT scan, the addition of one of these MR sequences instead of CT reduces patient movement, cost to

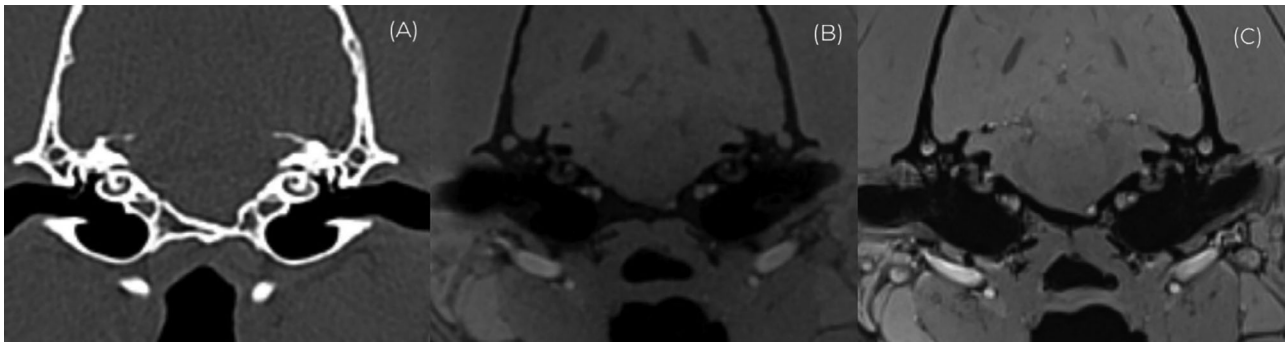

FIGURE 5 | An example of how it was difficult to measure cortical margins of the tympanic bulla with the UTE and VIBE sequences because of the interface between gas in the tympanic cavity and the adjacent cortical bone. A, CT. B, UTE MR image. C, VIBE MR image.

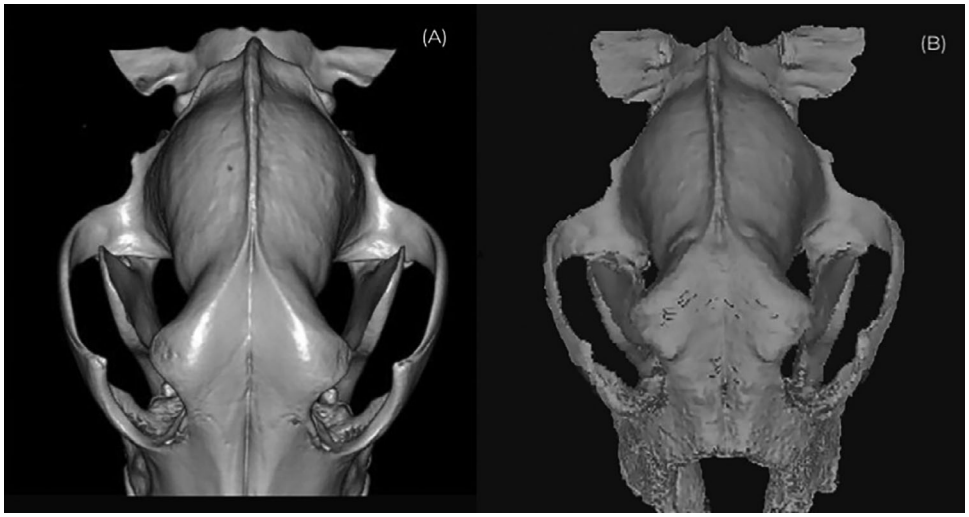

FIGURE 6 | A, 3D volume-rendered CT image. B, 3D volume-rendered UTE MR image.

the client, and radiation exposure to the patient and potential personnel while performing a complete assessment of both soft tissue and osseous structures. In some clinical settings, MR and CT scanners may be housed in different areas of the hospital or even have off-site MRI, so reducing patient transportation of often unstable patients would be preferable.

One advantage of CT is the ability to make 3D volume-rendered images rapidly. While 3D volume-rendered images can be generated from the UTE and ZTE MR sequences, currently, this postprocessing manipulation of the images cannot be generated at the workstation and requires time-intensive manipulation with postprocessing viewing software (Analyze 14.0, AnalyzeDirect, Inc., KD, USA). As such, extra time is involved in the creation of 3D reconstructions from these MR sequences, but it is feasible (Figure 6).

Our study has a few limitations. First, both CT and MR images were acquired approximately 2 months apart. However, since all the dogs in this study were full-grown adult dogs and served as their own control, it is highly unlikely that any osseous changes would occur during that time. Second, only healthy dogs were included in the study design since the purpose of this study was to optimize and validate short TE MR sequences for the assessment of cortical bone. Third, the UTE sequence is a Work in Progress sequence by Siemens and is currently not available for commercial or clinical use.

In conclusion, VIBE, PETRA, and UTE MR sequences have diagnostic image quality and provide consistent quantitative measurements and qualitative assessment of cortical bone and associated anatomy of the canine skull when compared with CT and were superior to standard T2W, PD, and T1W sequences. Any of the short TE MR sequences are viable options to incorporate into clinical protocols to further evaluate cortical bone and associated anatomy of the head while reducing patient transportation and client costs. The only structure in this study that was difficult to accurately assess was the tympanic bulla in the VIBE and UTE sequences. Further studies evaluating other anatomical regions and patients with pathology would be beneficial for further studies.

Acknowledgments

This work was supported by the Resident Research Grant from the American College of Veterinary Radiology's Veterinary CT/MR Society. The authors would like to thank research technician, Jocelyn Burkit, and MRI technician, Adam Harris, for their contributions in both technical

support and data acquisition, and James Robertson and Dr. Kim Love for statistical consultation and computation.

List of Author Contributions

Category 1

(a) Conception and design: Cicci, Cohen, Keenihan, Sommer

(b) Acquisition of data: Cicci, Cohen, Keenihan, Bailey, Graham

(c) Analysis and interpretation of data: Cicci, Cohen, Keenihan

Category 2

(a) Drafting the article: Cicci, Cohen, Keenihan, Sommer, Bailey, Graham

(b) Revising article for intellectual content: Cicci, Cohen, Keenihan, Sommer, Bailey, Graham

Category 3

(a) Final approval of the completed article: Cicci, Cohen, Keenihan, Sommer, Bailey, Graham

Category 4

(a) Agreement to be accountable for all aspects of the work in ensuring that questions related to the accuracy or integrity of any part of the work are appropriately investigated and resolved: Cicci, Cohen, Keenihan, Sommer, Bailey, Graham

Conflicts of Interest

The authors declare no conflicts of interest.

Previous Presentation or Publication Disclosure

Data from this study were previously presented and published under the abstract "Comparison of VIBE, PETRA, and UTE MRI sequences and standard T2W, PD, and T1W MRI sequences with CT for evaluation of the canine skull" at the 2021 Virtual American College of Veterinary Radiology Annual Scientific Meeting.

EQUATOR Network Disclosure

An EQUATOR network checklist was not used.

Addendum 1. Osseous Structures and Imaging Planes for Quantitative Measurements

- **Overall bone thickness**
  - Bilateral temporal process of the zygomatic bone, mediolateral measurement at the widest part just ventral to the temporozygomatic suture, transverse plane
  - Bilateral pterygoid bone, mediolateral measurement mid-aspect of the bone at the widest part, transverse plane
  - Bilateral squamous part of the frontal bone, dorsoventral measurements at both rostral and caudal aspects at the thickest part, transverse plane
  - Bilateral body of the mandible, perpendicular to the bone at the widest part, transverse plane
  - External sagittal crest of the occipital bone, mediolateral measurement at the widest part of the base, transverse plane
  - External sagittal crest of the parietal bone, dorsoventral measurement at the level of the sagittal suture, transverse plane
  - Basisphenoid bone, dorsoventral measurement, dorsum sellae to the base of the body of the basisphenoid bone, sagittal plane
  - Basisphenoid bone, dorsoventral measurement, transverse plane
  - External occipital protuberance of the occipital bone, rostrocaudal measurement at the widest part, sagittal plane
  - Bilateral zygomatic process of the temporal bone, mediolateral measurement, at the widest part of the ventral aspect, dorsal plane
  - Bilateral zygomatic process of the temporal bone, perpendicular to the bone at the widest part at the level of the temporomandibular joint, transverse plane
  - Bilateral coronoid process of the mandible, mediolateral measurement, at the widest part, dorsal plane
  - Bilateral tympanic bulla wall thickness, dorsoventral measurement at the medial aspect of the bulla, dorsal and transverse plane
  - Bilateral tympanic inner cavity, dorsoventral measurement, mid-aspect of the ventral wall at the level of the cochlea, transverse plane
  - Bilateral condylar process of the mandible, rostrocaudal measurement at the level of the temporomandibular joint, dorsal plane
  - Bilateral condylar process of the mandible, perpendicular to the bone at the widest part at the level of the temporomandibular joint, transverse plane
  - Bilateral pterygoid, mediolateral measure just rostral to the pterygoid process, dorsal plane
  - Bilateral occipital condyle, mediolateral measurement at the widest part at the junction of the adjacent skull, dorsal and transverse planes
- **Intracranial dimensions**
  - Cranial height, dorsoventral measurement, from the external sagittal crest of the parietal bone to the basilar part of the occipital bone, transverse plane
  - Cranial width, mediolateral measurement at the widest part, transverse plane
  - Intracranial height, internal lamina ventrally to the Sella turcica, just rostral to the dorsum sellae, sagittal plane
  - Intracranial length, cribriform plate caudally to the foramen magnum, sagittal plane
  - Intracranial length, cribriform plate caudally to the vermiform impression of the occipital bone, dorsal plane
  - Cranial width, mediolateral measurement at the widest part, dorsal plane
- **Foraminal assessment**
  - Bilateral oval foramen, inner and outer widths at the largest dimensions, transverse plane
  - Foramen magnum, outer width measurement from the right occipital condyle to the left occipital condyle, transverse and dorsal planes
  - Foramen magnum, dorsoventral measurement at the caudal most aspect of the occipital bone parallel to the base of the skull, sagittal plane

Addendum 2. Osseous Structures and Imaging Planes for Qualitative Assessment

- **Overall bone thickness**
  - Bilateral visibility of corticomedullary definition of the body of the mandible and distinction between bone and adjacent soft tissue structures/gas, transverse plane
  - Bilateral visibility of cortical margins of the coronoid process of the mandible, transverse plane
  - Bilateral visibility of cortical margins of the condylar process of the mandible, transverse and dorsal planes
  - Visibility of cortical margins of the basisphenoid bone, transverse plane
  - Bilateral visibility of the cochlea, transverse plane
  - Visibility of corticomedullary definition of the external occipital protuberance of the occipital bone, transverse plane
  - Bilateral visibility of the tympanic bullae for the distinction between bone and adjacent soft tissue structures/gas, transverse and dorsal planes
- **Foraminal assessment**
  - Bilateral visibility of the optic canal, transverse plane
  - Bilateral visibility of the oval foramen, transverse plane

References

1. S. B. Cho, H. J. Baek, K. H. Ryu, et al., "Clinical Feasibility of Zero TE Skull MRI in Patients With Head Trauma in Comparison With CT: A Single-Center Study," *Ajnr American Journal of Neuroradiology* 40, no. 1 (2019): 109–115.

2. J. Du, M. Carl, M. Bydder, A. Takahashi, C. B. Chung, and G. M. Bydder, "Qualitative and Quantitative Ultrashort Echo Time (UTE) Imaging of Cortical Bone," *Journal of Magnetic Resonance* 207 (2010): 304–311.

3. A. Gallastegui, E. Davies, A. L. Zwingenberger, S. Nykamp, M. Rishniw, and P. J. Johnson, "MRI Has Limited Agreement With CT in the Evaluation of Vertebral Fractures of the Canine Trauma Patient," *Veterinary Radiology & Ultrasound: The Official Journal of the American College of Veterinary Radiology and the International Veterinary Radiology Association* 60, no. 5 (2019): 533–542.

4. E. Koh, E. R. Walton, and P. Watson, "VIBE MRI: An Alternative to CT in the Imaging of Sports-related Osseous Pathology?," *Bjr* 91, no. 1088 (2018): 20170815.

5. C. Lee, K. J. Jeon, S. S. Han, et al., "CT-Like MRI Using the Zero-TE Technique for Osseous Changes of the TMJ," *Dento Maxillo Facial Radiology* (2019): 20190272.

6. R. E. Breighner, Y. Endo, G. P. Konin, L. V. Gulotta, M. F. Koff, and H. G. Potter, "Technical Developments: Zero Echo Time Imaging of the Shoulder: Enhanced Osseous Detail by Using MR Imaging," *Radiology* 286, no. 3 (2018): 960–966.

7. R. E. Breighner, E. A. Bogner, S. C. Lee, M. F. Koff, and H. G. Potter, "Evaluation of Osseous Morphology of the Hip Using Zero Echo Time Magnetic Resonance Imaging," *American Journal of Sports Medicine* 47, no. 14 (2019): 3460–3468.

8. G. Delso, F. Wiesinger, L. I. Sacolick, et al., "Clinical Evaluation of Zero-Echo-Time MR Imaging for the Segmentation of the Skull," *Journal of Nuclear Medicine* 56, no. 3 (2015): 417–422.

9. D. M. Grodzki, P. M. Jakob, and B. Heismann, "Ultrashort Echo Time Imaging Using Pointwise Encoding Time Reduction With Radial Acquisition (PETRA)," *Magnetic Resonance in Medicine* 67, no. 2 (2012): 510–518.

10. M. D. Robson and G. M. Bydder, "Clinical Ultrashort Echo Time Imaging of Bone and Other Connective Tissues," *Nmr in Biomedicine* 19, no. 7 (2006): 765–780.

11. Y. H. Lee, J. S. Suh, and D. Grodzki, "Ultrashort Echo (UTE) versus Pointwise Encoding Time Reduction With Radial Acquisition (PETRA) Sequences at 3 Tesla for Knee Meniscus: A Comparative Study," *Magnetic Resonance Imaging* 34, no. 2 (2016): 75–80.

12. C. Westbrook, et al., *MRI in Practice*. 4th ed. (John Wiley & Sons, 2011).